N87-26010

DESIGN APPLICATIONS FOR SUPERCOMPUTERS

C. J. STUDERUS
GENERAL ELECTRIC COMPANY
CINCINNATI, OHIO

ABSTRACT

The complexity of codes for solutions of real aerodynamic problems has progressed from simple two-dimensional models to three-dimensional inviscid and viscous models. As the algorithms used in the codes increased in accuracy, speed and robustness, the codes were steadily incorporated into standard design processes. The highly sophisticated codes, which provide solutions to the truly complex flows, require computers with large memory and high computational speed. The advent of high-speed supercomputers, such that the solutions of these complex flows become more practical, permits the introduction of the codes into the design system at an earlier stage. The purpose of this paper is to present the results of several codes which either have already been introduced into the design process at GE-AEBG or are rapidly in the process of becoming so. The codes fall into the area of turbomachinery aerodynamics and hypersonic propulsion. In the former category, results are presented for three-dimensional inviscid and viscous flows through nozzle and unducted fan bladerows. In the latter category, results are presented for two-dimensional inviscid and viscous flows for hypersonic vehicle forebodies and engine inlets.

INTRODUCTION

At the General Electric Aircraft Engine Business Group (GE-AEBG), aerodynamic computer codes have been developed over the past thirty years to provide solutions for flows through a large variety of turbomachinery and propulsion systems. The capability of these codes has progressed from providing the solutions of simple two-dimensional inviscid meridional and blade-to-blade flows, and viscous boundary-layer flows, to the solutions of full three-dimensional inviscid and viscous flows. As the algorithms used in the codes increased in accuracy, speed, and robustness, the codes were steadily incorporated into standard design processes. However, the highly sophisticated codes which provide solutions to the full complexity of three-dimensional flows require computers with very large memory and extremely high computational speed. Therefore, it was not until the availability of such high-speed supercomputers that the solutions of these complex flows became more practical and permitted the introduction of these advanced codes into the design process at earlier and earlier stages. The advantage of being able to utilize these codes as design tools was one of the factors which prompted GE to purchase its own supercomputer, a CRAY-XMP.

The purpose of this paper is to present the results of several such codes which either have already become a part of the design process at GE-AEBG or are rapidly in the process of becoming so. The codes fall into two specific fluid dynamic areas: turbomachinery aerodynamics and hypersonic propulsion.

TURBOMACHINERY AERODYNAMICS

The actual flow through a turbomachinery bladerow is exceedingly complex. It is unsteady, compressible and viscous, producing strong three-dimensional effects, as indicated schematically in Figure 1. When the incoming endwall boundary layer encounters the leading edge, it rolls up to produce a so-called horseshoe vortex, which wraps around the leading edge. One leg of this vortex is convected along the suction surface. The other leg is convected across the passage to the suction surface of the opposite bladerow. The boundary layers farther along the endwalls are forced from the pressure surfaces of the blades to the suction surfaces by the cross-passage pressure gradients. They are deflected in the spanwise direction and roll up into a passage vortex. Similarly, when the endwall boundary layer flows into the corner and interacts with the boundary layer on the suction surface, corner vortices are produced. Trailing vortices result from vortex sheets created by a varying circulation along the blade span and from interaction of the different velocities over the pressure and suction surfaces. Tip clearance flows are created when the undeflected throughflow across the clearance gap combines with the flow caused by the pressure difference between pressure and suction surfaces. The relative motion between a blade and the casing boundary layer result in scraping and skewing effects. Finally, blade wakes produce viscous mixing after the trailing edges.

Efficient design of turbomachinery bladerows, especially in the transonic regime, requires accurate evaluation of these phenomena. The aerodynamic design starts with a two-dimensional circumferentially averaged solution in which the flow path is defined and the bladerows are modelled in terms of blade loadings, losses, and thickness distributions. This is followed by two-dimensional blade-to-blade analyses at several spanwise locations in order to design custom-tailored airfoil shapes that will produce the desired circumferentially averaged flow field. Additional analyses account for secondary flow effects. The blade shapes obtained are then

evaluated by means of a three-dimensional code, which provides a single unified solution for the design. Modifications to the blade shapes and flow path can then be made on the basis of additional three-dimensional solutions to achieve the final design of the bladerow.

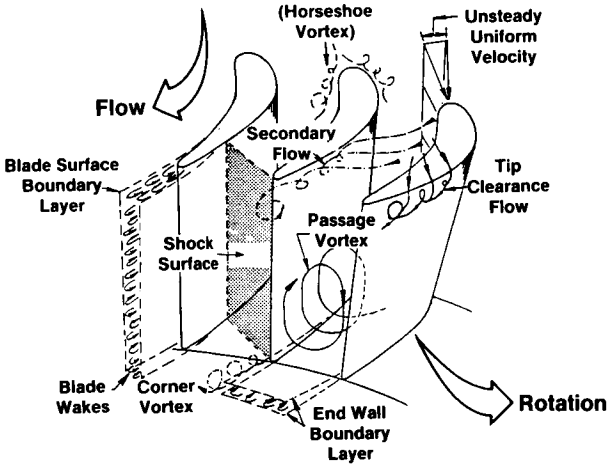

Figure 1. Complex Flow Phenomena in Turbomachinery.

Inviscid 3-D Nozzle Flow

A great deal of useful design information about the structure and general characteristics of turbomachinery flows can be obtained from three-dimensional inviscid analyses. The inviscid flow determines the pressure distributions on the blade surfaces, except for regions of local flow separation, and can be used to evaluate many of the features of the secondary flows produced in the bladerow passage. Therefore, the final design of conventional bladerows are now carried out with the use of a three-dimensional inviscid Euler Code, EULER3D, developed by Dr. D. G. Holmes[1] at the GE Research and Development Center (GE-R&DC). The algorithm used in that code is based on a scheme developed by Jameson, et al.[2] The Euler equations are discretized in space using a straightforward finite-volume scheme that is equivalent to central spatial differencing on a regular, rectangular grid. The discretized equations are marched forward in time to a steady state using an explicit, four-step, Runge-Kutta scheme. Some smoothing is needed to suppress wiggles and to capture shocks. Both smoothing tasks are fulfilled by a blend of second and forth-order smoothing.

The following results, taken from Reference 3, present the flow through the first-stage nozzle of a low-pressure turbine with non-cylindrical endwalls, for which experimental data was available in the form of traverses of total pressure just downstream of the trailing edge. Due to the long passage between the upstream high-pressure turbine and the low-pressure turbine, relatively thick boundary layers were present at the nozzle entrance, as indicated by total-pressure traverses taken there. To investigate the secondary flows produced in the nozzle by these thick boundary layers, an inlet profile of total pressure, based on the measured data, was specified for the computation. The three dimensional grid used had 66825 nodes, 25 in the tangential, 33 in the radial, and 81 in the axial directions, Figure 2. A three-dimensional representation of the nozzle passage is shown in Figure 3. A completely converged solution requiring approximately 900 iterations could be obtained in 9 hours on an IBM Model 3080, or in approximately 15 minutes on a CRAY-XMP. A solution sufficiently converged for design purposes could be obtained in half that time.

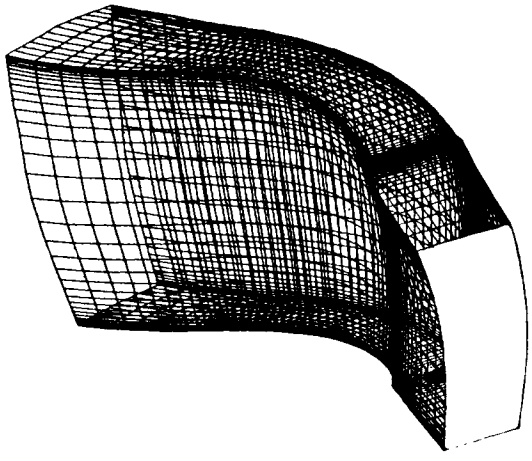

Figure 2. Grid for Inviscid Nozzle Flow Computation.

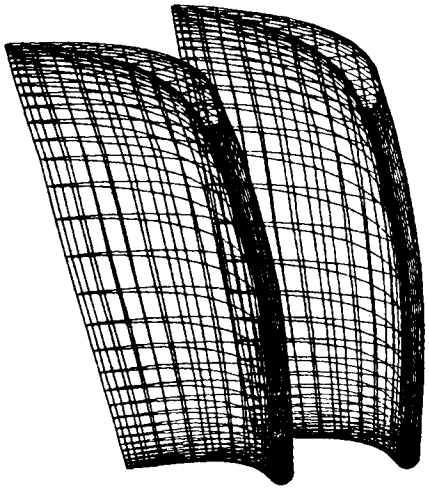

Figure 3. Grid Representation of Nozzle Bladerow.

The formation of the secondary flow is shown by the streamline traces on the casing endwall and blade surfaces, Figures 4 through 6. On the casing endwall, the flow is swept toward the suction surface by the action of the cross-passage pressure gradient on the low momentum fluid near the endwall. The non-cylindrical endwalls produce generally radially outward flow in the entire passage. However, superposed on this are the radial flows due to the passage secondary flow. On the pressure surface, the secondary radial flows are from pitchline toward each endwall; on the suction surface, the secondary radial flow is toward the pitchline.

The generation of the corner vortex is shown by tracing the location of particles in several blade-to-blade streamsheets near the tip, Figure 7. As the flow progresses from leading

edge to trailing edge and downstream, the particles near the suction surface are generally swept radially inward, while those originating on the pressure side are swept across the passage along the tip.

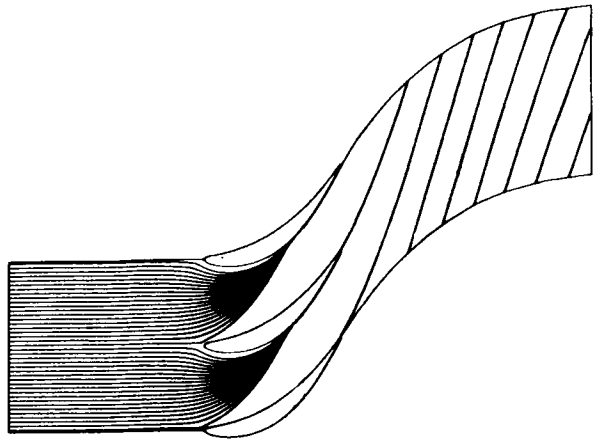

Figure 4. Inviscid Streamlines on Nozzle Endwall.

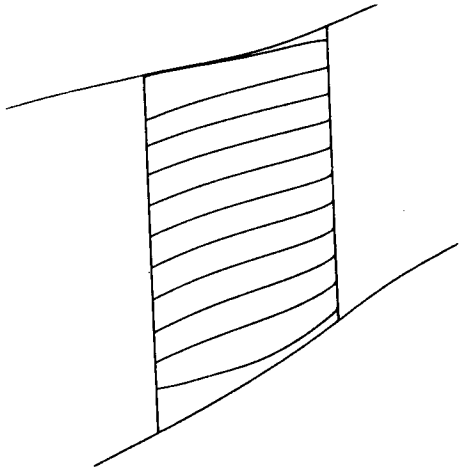

Figure 5. Inviscid Streamlines in Nozzle Pressure Surface.

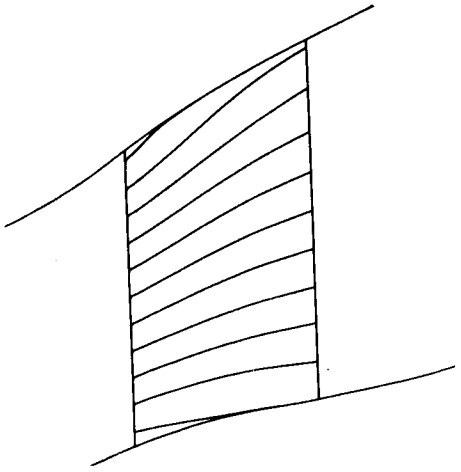

Figure 6. Inviscid Streamlines in Nozzle Suction.

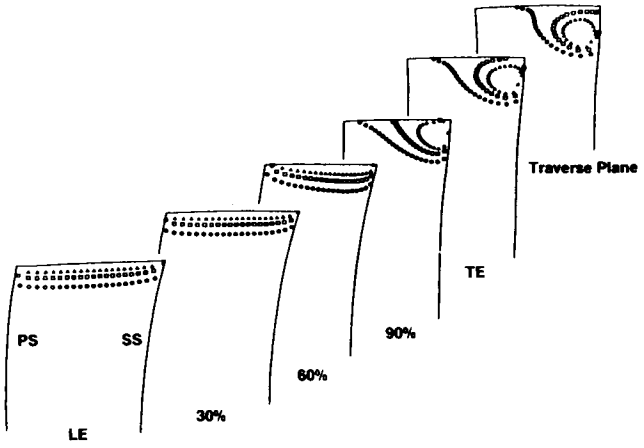

Figure 7. Streamline Traces Through Nozzle Passage.

For this bladerow, contours of exit total pressure had been produced from experimental data. The calculated values are compared in Figure 8. The presence of the secondary flow vortex is clearly demonstrated. Since the inviscid computation has no provision for blade boundary layers or mixing downstream of the trailing edge, no wake effects are produced.

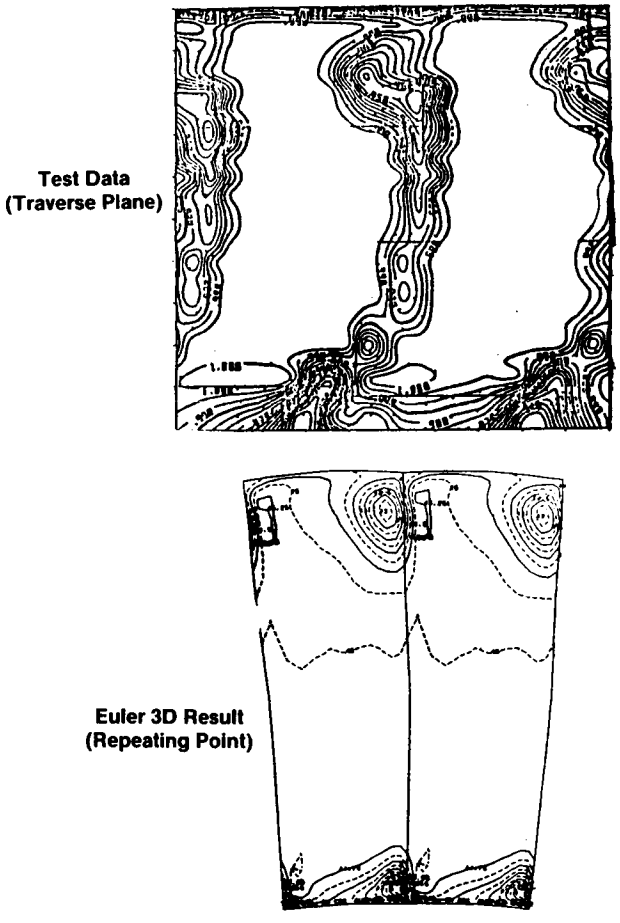

Figure 8. Comparison of Computed and Measured Contours of Total Pressure.

Viscous 3-D Nozzle Flow

Although inviscid solutions can indicate many of the features of real turbomachinery flows, viscous analyses are required to evaluate local regions of separated flows, frictional forces, heat transfer, wake effects, etc. For most turbomachinery applications, these phenomena must be evaluated in environments of high Reynolds number with thin turbulent boundary layers. This places a large burden on the analysis in the form of very dense grid requirements in regions of high shear along the blade and endwall surfaces.

A three-dimensional viscous turbomachinery code has been developed at GE. Although the code is not yet a part of the design system, the availability of a supercomputer, with its number-crunching power and memory capacity, is accelerating the transition of the code into the design process. The HAH code,[4] developed by Dr. C. Hah at the GE-R&DC is a fully elliptic, compressible, turbulent, viscous flow program capable of calculating the three-dimensional flow inside a cascade of airfoils at design and off-design conditions. The Reynolds-averaged Navier-Stokes equations are solved together with either an algebraic Reynolds-stress turbulence model or a two-equation (k-ϵ) turbulence model. The finite-difference formulation is based on the control-volume methodology of Patankar and Spalding in which a pressure-correction equation is solved along with the governing equations. The fluid dynamic conservation equations and the transport equations for the turbulent quantities are solved sequentially on a staggered grid. The highly non-linear and coupled set of equations are solved on the grid nodes with an iterative method of solution, using an upwind discretization scheme for the convective terms.

Viscous solutions have been obtained for the same nozzle bladerow previously described for the EULER3D application. The results presented here were obtained by Dr. Hah, and documented by J. Leylek.[5] A fine grid was used, comprised of 64260 nodes, 36 in the tangential, 35 in the radial, and 51 in the axial directions. Figures 9, 10, and 11 show the grid patterns in the blade-to-blade, crossflow, and meridional planes, respectively. The solution was obtained on an IBM model 3080 mainframe computer, using double precision. Starting from a uniform flow condition, 2000 iterations were required to obtain a converged solution. The computation took approximately 70 hours of CPU time.

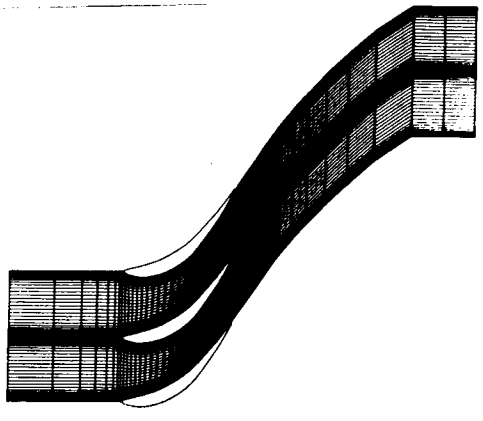

Figure 9. Blade-to-Blade Grid for 3D Viscous Calculations.

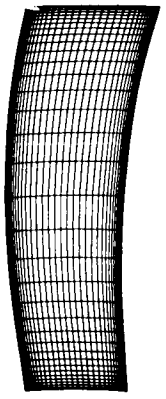

Figure 10. Crossplane Grid for 3D Viscous Calculations.

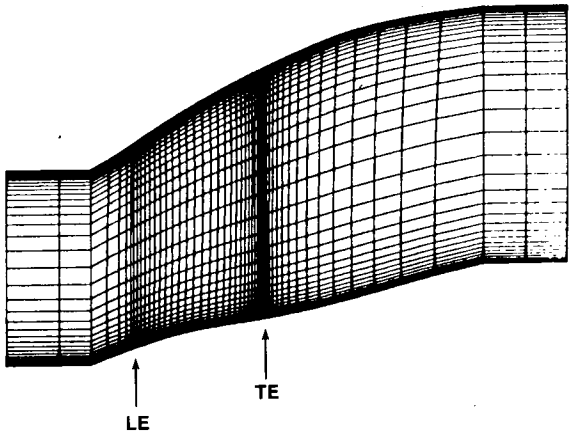

Figure 11. Meridional Grid for 3D Viscous Calculations.

The total-pressure contour levels at 0.5 percent increments are compared to the experimental data at the downstream measurement plane, Figure 12, and show good qualitiative and quantitative agreement with the data. The existence of the loss region near the outer wall is properly simulated in the computational results. However, the overall predicted wake region is larger than the measured wake. This is due to "artificial viscosity" created by the numerical scheme which is added to the molecular and eddy viscosity mechanisms naturally present in the flow field. The radial distribution of the mass-weighted, circumferentially averaged and normalized total pressure is compared to the experimentally measured data in Figure 13. This figure shows the presence and the extent of the predicted loss region near the tip with respect to the measured losses. The computed results do not exhibit the rapid recovery at the tip. However, there is excellent agreement over 85 percent of the span, which confirms the excellent comparison between computations and experiments seen in Figure 12.

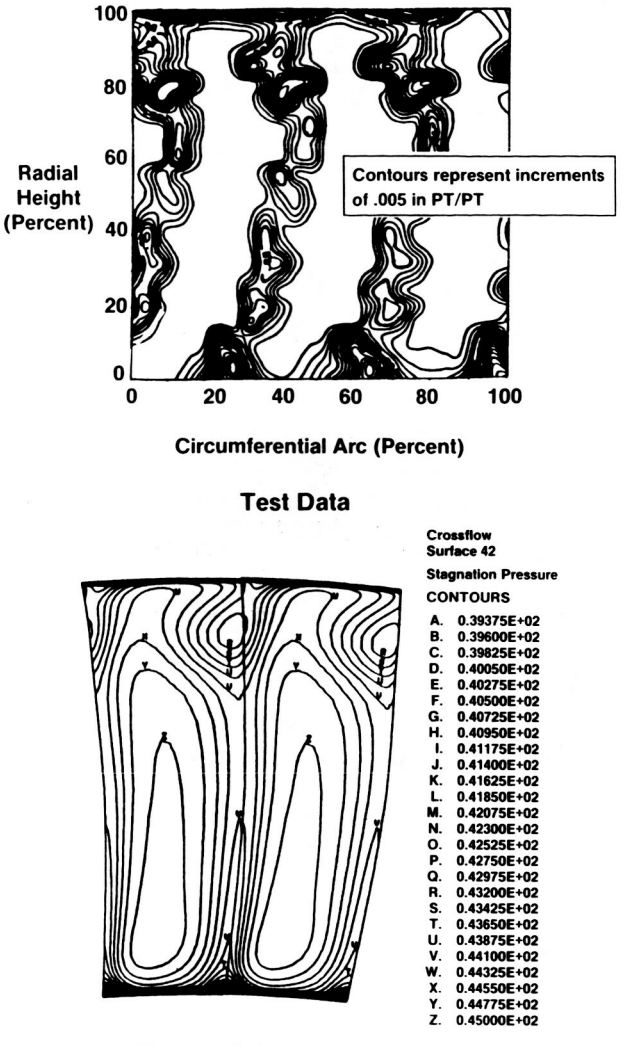

Figure 12. Comparison of Computed and Measured Contours of Total Pressure.

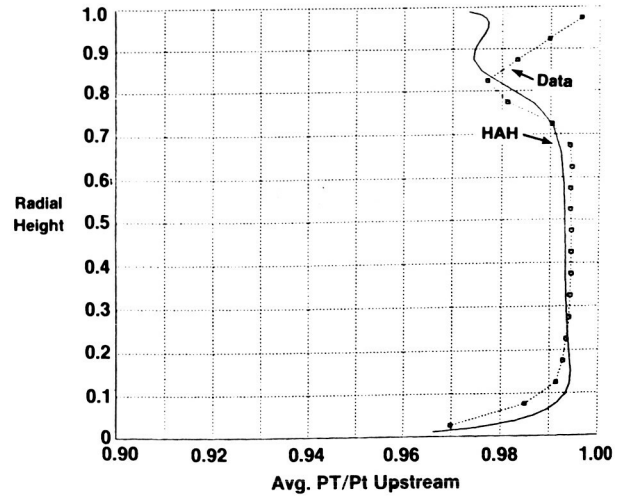

Figure 13. Radial Distributions of Circumferentially Mass-Averaged Total Pressure.

The following set of plots were included in Reference 5 to describe and to help verify the computed flow field. Figures 14 and 15 show the velocity vectors and the streamline pattern near the suction surface. Figure 16 is a photograph of the streamline pattern obtained on the suction surface near the stator exit area. This pattern was obtained in a flow visualization experiment using lampblack and oil traces. A careful examination of the vector plot in Figure 14 shows that the downward direction of the vectors near the outer wall agree well with the observed flow pattern in Figure 16. The region where the flow appears to move toward the pitchline corresponds to the high loss section in the total-pressure plot of Figure 13. The endwall streamlines, near the inner and outer endwall surfaces, are shown in Figures 17 and 18, respectively. Photographs of the streamline patterns on the endwall surfaces from the flow visualization experiments, Figures 19 and 20, substantiate the predicted patterns shown in Figures 17 and 18.

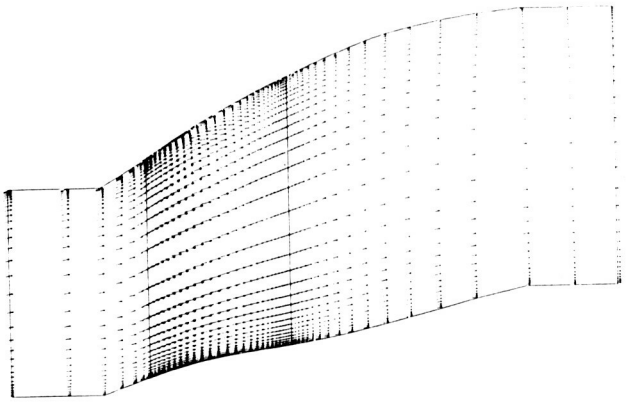

Figure 14. Velocity Vectors in Meridional Plane Near Suction Surface.

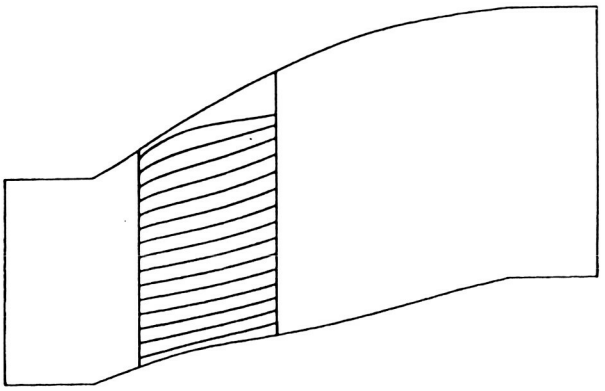

Figure 15. Streamline Pattern Near Suction Surface.

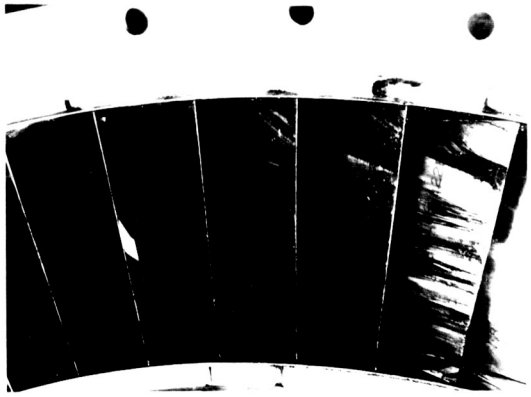

Figure 16. Photograph of Flow Traces on Aft Suction Surface.

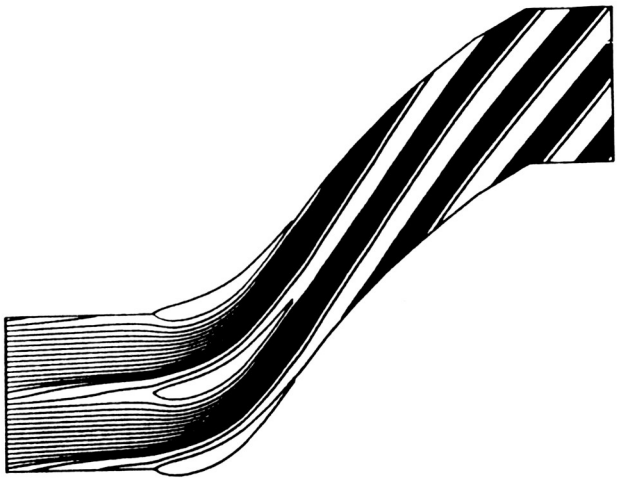

Figure 17. Streamline Pattern Near Hub Surface.

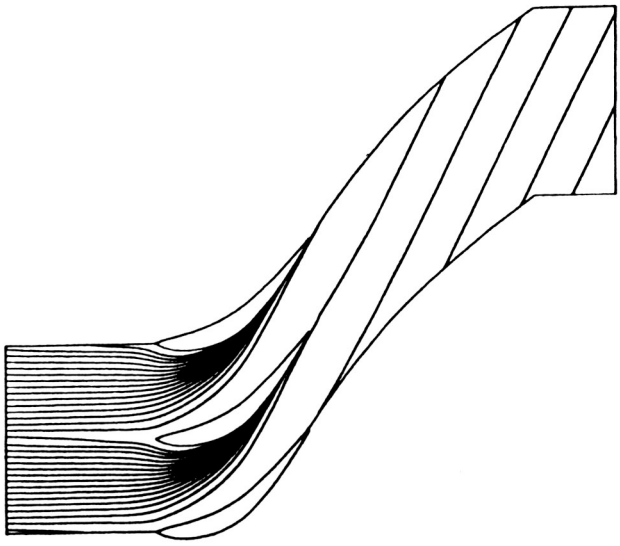

Figure 18. Streamline Pattern Near Tip.

Figure 19. Photograph of Flow Traces on Inner Endwall Surface.

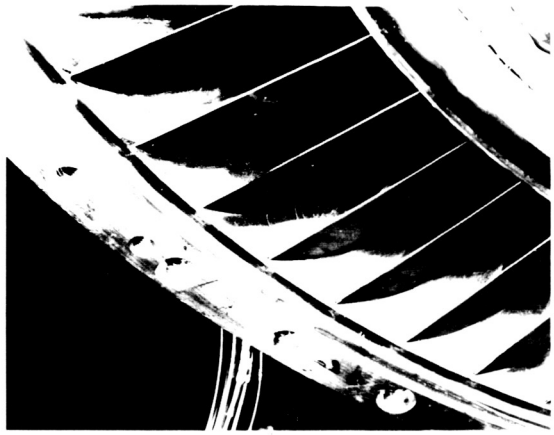

Figure 20. Photograph of Flow Traces on Outer Endwall Surface.

Inviscid 3-D Unducted Fan Flow

Propfan engines can provide much greater mass flows than those of modern turbofans, thus providing the potential for greater propulsive efficiency. NASA's Advanced Turboprop Program is aimed at establishing the technology for single-rotation and double-rotation propfan engines. Large fuel savings have been estimated for single-rotation propfan configurations; even greater savings are estimated for advanced counter-rotation designs. The GE Unducted Fan Engine (UDF™), Figure 21, has such a counter-rotation design, in which the blades rotate at the same speed, but in opposite directions.

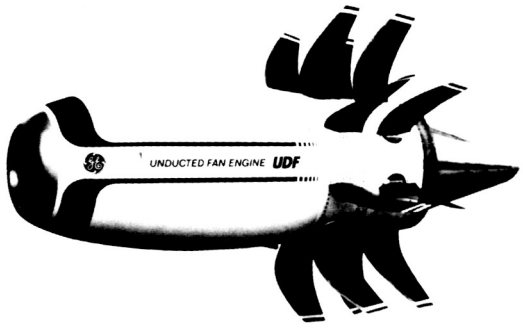

Figure 21. General Electric Unducted Fan Engine.

Current aerodynamic design of the GE-UDF™ follows the same general procedure as for conventional bladerows, described previously. That is, a circumferentially averaged flow field solution is obtained, with suitably prescribed chordwise and spanwise loadings, losses, and blockage. This is followed by two-dimensional blade-to-blade and secondary flow analyses to determine the basic blade shapes. The resulting propfan bladerows are then analyzed with the EULER3D code to produce the final design. The EULER3D code has been modified to handle the far-field boundary conditions beyond the bladerow tips.

For the case of counter-rotating unducted fans, the design should include the interaction between the two bladerows. The approach presently utilized is to analyze one bladerow in detail, with the effects of the other bladerow simulated by axisymmetric source terms in the three-dimensional equations. Mass sources in the continuity equation simulate the effects of blade blockage; force terms in the momentum equations simulate the turning in the adjacent bladerow; work terms in the energy equation represent the conservation of enthalpy simultaneously. The source terms are computed by performing an axisymmetric analysis of the flow through the primary and secondary bladerows. This axisymmetric solution is passed to the Euler solver as a starting solution and the Euler source terms are calculated as the residuals of the initial solution. Thus, each bladerow can be designed separately, assuming only that the other bladerow meets its design intent. Either upstream or downstream bladerows can be simulated in this manner.

Results are shown in Figures 22 and 23 for the EULER3D solutions of each of the bladerows of a counter-rotating UDF™ at a flight Mach number of 0.72. Figure 22 presents the contours of local Mach number on the forward rotating bladerow, which include the fluid dynamic effects of the aft rotating bladerow. The location of the aft bladerow is indicated in the figure by the darkest band on the hub surface. For this solution, the aft bladerow is, of course, represented by axisymmetric source terms. Similarly, Figure 23

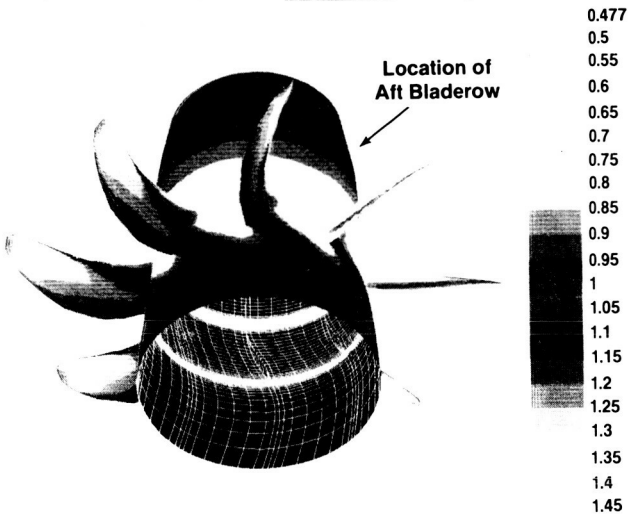

Figure 22. Contours of Local Mach Number on Forward UDF™ Bladerow.

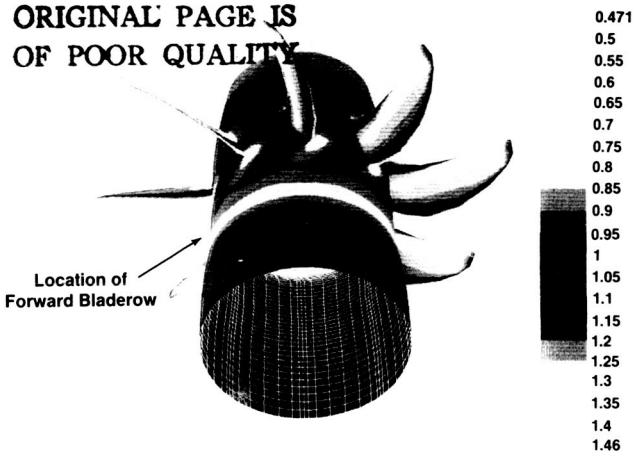

Figure 23. Contours of Local Mach Number on Aft UDF™ Bladerow.

presents the contours of local Mach number on the aft rotating bladerow, which include the effects of the forward bladerow. The location of the forward bladerow is indicated in that figure by the lightest band on the hub surface. High supersonic Mach numbers are present in the tip regions of both bladerows and extend almost to the hub on the aft bladerow. Although the bladerows being simulated in these solutions are represented in the analysis by axisymmetric terms, the bladerows being analyzed produces periodic flow effects in the region occupied by the simulated bladerows, as can be faintly seen by the varying width of the lightest band in Figure 23. An indication of the computational grid used for the calculations is shown on the inside surfaces of the hub. The grid consisted of 41905 nodes, 17 in the tangential, 29 in the radial, and 85 in the axial directions. The computation time for each bladerow solution was 5 minutes on a CRAY-XMP.

HYPERSONIC PROPULSION

There has been a resurgence of interest in SCRAMJET technology as the feasibility of hypersonic propulsion is re-examined. One of the factors that has been put forth as a key improved technology which can lead to successful design of hypersonic vehicles and engines is the availability of new sophisticated computational codes. These codes will provide detailed solutions to the complex flow problems which must be solved. The full Navier-Stokes equations can be solved in one form or another to analyze the internal and external flows involved. The supercomputers required to run these codes in an efficient manner are now available. An effort is underway at GE-AEBG to implement such codes in a suitable design system. The following sections illustrate the type of design problems involved in the design of engine inlets and some of the codes currently being actively pursued by GE-AEBG.

Vehicle Forebody Flows

The performance of a hypersonic propulsion engine is greatly dependent upon the vehicle forebody, since it determines the amount of air captured and the efficiency of that process. The forebody provides a system of ramps which produce external shocks to compress the air prior to

ingestion into the engine inlet. The compression efficiency is degraded by shock losses, wall shear, and heat loss. Therefore, the shock layer properties of the forebody must be accurately determined, including the effects of local phenomena. Since the leading edge must have finite bluntness, a region of subsonic/transonic flow is produced with the attendent features of vorticity and entropy swallowing. Along the compression surface, there are real-gas effects, transition of the boundary layer to turbulent flow, with high-Mach-number effects which should be included in the turbulence model. At the compression corners, there is always the possibility of boundary-layer separation. The surface effects, of course, influence the vehicle design. The surface heating determines the cooling requirements, and the surface friction and pressure contribute to the force balance.

Many codes have been, and continue to be, developed to analyze these flows, ranging from coupled inviscid/boundary-layer codes, to Parabolized Navier-Stokes (PNS) codes, to full Navier-Stokes codes. Several of these are being evaluated by GE-AEBG. One is the so-called SCRAMP code, developed by SAIC.[6] This is a PNS code which requires significantly less computer capacity and computational time than an elliptic code, and is therefore more advantageous as a design tool. The code uses the linearized implicit algorithm of Beam and Warming, the near-wall subsonic layer treatment of Schiff and Steger, either the Baldwin-Lomax or two equation k-ϵ turbulence model, and a fitted bow shock. The upstream influence of the flow can be accounted for by global pressure iteration. For blunt-nosed bodies, the space-marching procedure is initiated from a viscous shock layer solution produced by the VSL code.[7]

Some typical results from the SCRAMP code are shown in Figures 24 and 25. Calculations were made for a two-dimensional laminar flow over a blunted double-ramp forebody at a flight Mach number of 18. The computations were made with 75 grid points across the shock layer and took approximately 3 minutes on the CRAY XMP. For this case, no separation occurred at the second ramp. Profiles of properties across the shock layer are shown at axial locations just ahead of the second ramp and at the entrance to the inlet. In the figure, the profiles at point A are shown as solid lines, with the thickness of the shock layer indicated by the height yA. With the exception of the viscous effects near the ramp surface, the profiles are uniform. The profiles at point B are shown as dashed lines. The shock layer at that point is considerably thinner due to the additional compression of the second ramp. Point B is also downstream of the intersection of the bow shock and the secondary shock produced by the second ramp. The intersection of the two shocks produces an expansion fan within the shock layer, in addition to the resultant downstream shock. This causes variations in the inviscid portions of the shock layer near the shock. The results of such a solution are then used to determine the mass flow and state of the air entering the inlet. Of particular interest for inlet design are the variations of η_{KE}, the kinetic energy efficiency, shown in Figure 25.

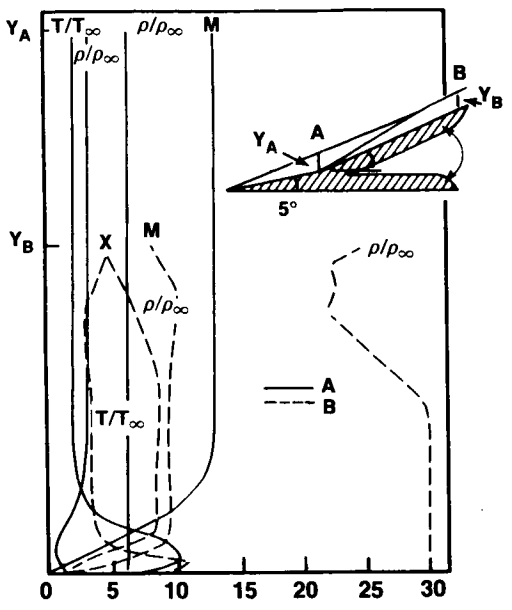

Figure 24. Profiles of Shock-Layer Properties on a Double-Ramp Forebody.

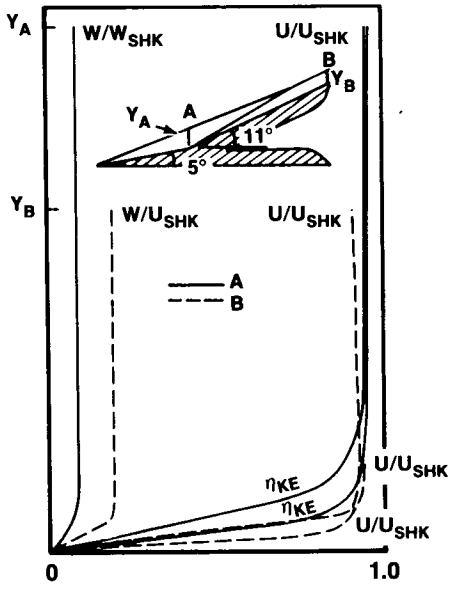

Figure 25. Profiles of Shock-Layer Velocities and Kinetic-Energy Efficiency.

Engine Inlet Flows

The engine inlet provides additional compression of the air to some minimum cross-section or throat and presents its own set of flow problems. The cowl leading edge produces an additional bow shock, which ultimately impinges on the ramp surface, producing a strong shock/boundary-layer interaction, possibly causing local separated flow. In addition, there is the existence of the corner flows due to the inlet sideplates and the possibility of local effects due to boundary-layer bleed. The inlet solution provides knowledge of the flow conditions at the throat and the losses produced by the shocks and viscous effects. This information is required for the engine cycle and performance calculations. And, just as for the

forebody, the surface heating determines the engine cooling requirements, while the surface friction and pressure contribute to the force balance.

Although the internal flow is really three-dimensional, analysis of even a two-dimensional simplification of an inlet flow requires sophisticated flow field codes. Among those being evaluated are the SAIC SCRINT code,[6] the NASA/Lewis PEPSIS[8] code, the NASA/Langley NASCRIN code,[9] and an Euler code called TRIAD2D.[10] The SCRINT code is the internal-flow equivalent of the SCRAMP code, i.e., a space-marching PNS code, which relies on profiles of initial data at the inlet entrance, obtained, for example, from a SCRAMP solution. PEPSIS is a three-dimensional supersonic viscous marching analysis for the flow over the forebody and through the inlet.

The NASCRIN code utilizes the time-dependent finite-difference method to solve the full Navier-Stokes equations in conservation form, using the explicit, predictor-corrector method of MacCormack for the solution algorithm and the algebraic, two-layer eddy viscosity model of Baldwin and Lomax for calculations of turbulent flow. An illustration of the results from the NASCRIN code are presented in Figure 26 for a two-dimensional inlet. This perfect-gas solution was computed for a uniform flow along the ramp surface at a Mach number of 5; no initial ramp boundary layer was assumed. The computation, which used a 55 x 61 grid, required 2574 cpu-seconds for 60,000 iterations on the CRAY-XMP. The plot of the flow vectors indicates the grid locations. The contours of Mach number define the bow shock produced by the leading edge of the slightly blunted cowl, and the reflected shocks which occur downstream. The contours of static pressure provide a sharper picture of this shock structure. Although the contours of total pressure show the extent of the loss regions due to the surface boundary layers, they tend to smear out the shocks near the throat.

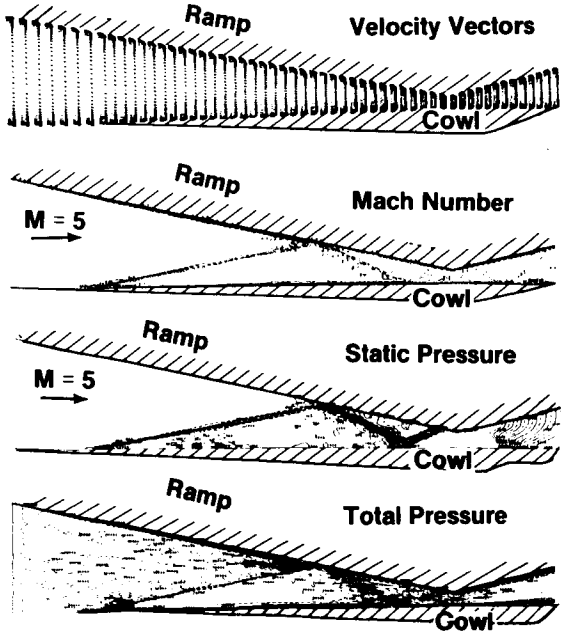

Figure 26. Contours of Inlet Flow Field Properties.

The TRIAD2D code, which is currently under development by Dr. D.G. Holmes at GE-R&DC, utilizes a method recently devised by A. Jameson.[11] This calculation procedure uses a triangular adaptive grid to build an unstructured network, one without a set of coordinates, by first connecting a set of points, working outward from each boundary surface. Where the patterns from adjoining surfaces meet, the code symmetrically removes excess points and reconnects them into a fairly regular triangular array. This method of building a grid has the advantage that grid points can easily be added to any region of the flow without disturbing the grid in other regions. In the TRIAD2D code, grid points are added in those regions where local gradients are highest, such as along shock waves.

The two-dimensional code currently solves only the Euler equations for a perfect gas. Results are shown for the flow in an inlet for which the entrance Mach number is 7.7. The calculation included the region of flow along the external surface of the cowl. The resulting grid, which was adaptively changed during the calculations, is shown in Figure 27. The solid black regions indicate the large number of grid points added in the regions where shock waves occur in the

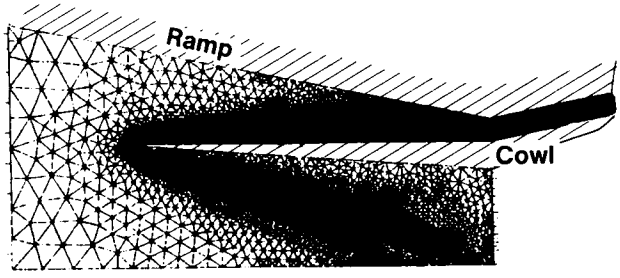

Figure 27. Triangular Grid for the TRIAD2D Code.

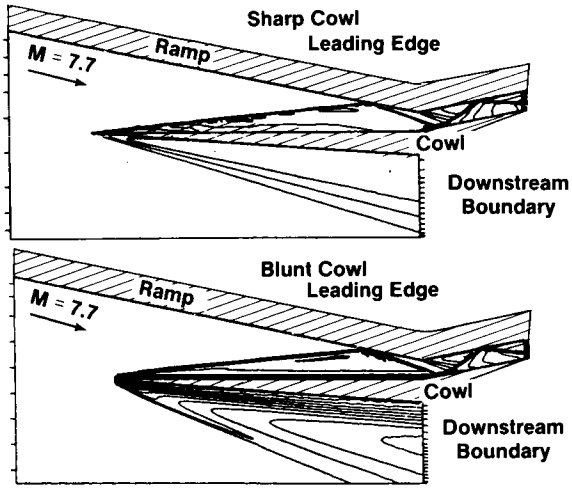

Figure 28. Inlet Contours of Mach Number.

internal flow and where expansion waves occur on the external cowl surface. The total number of grid points is 11991. Contours of Mach number are presented in Figure 28 for solutions with sharp and blunted cowl leading edges. The cowl shock and its reflection from the ramp are clearly shown in both cases. The solution for the blunted leading-edge, however, also shows a significant

variation in Mach number due to the entropy layer along the cowl inner surface . These solutions required approximately 1220 cpu-sec for 5070 iterations on the CRAY X-MP computer.

Although currently providing only an inviscid solution, the TRIAD2D code is another illustration, similar to the EULER3D code, of how a robust inviscid code can be a vital part of the design process by providing a complex flow solution in a rapid efficient manner. The shock locations and distributions of surface pressure are the paramount initial concerns in an inlet design, since they can indicate possible regions of flow separation. Rapid evaluation of candidate inlet geometries to achieve improved shock structure and strengths is enhanced by a code which requires minimum grid manipulation by the user. A unique feature of the TRIAD2D code is its adaptive grid which relieves the user of a priori specification of grid points in regions of interest whose location is not known beforehand.

SUMMARY

Supercomputers provide for more rapid development of complex aerodynamic codes and for faster introduction of the codes into the design process. The large storage capacity of these computers permits the user to specify grid sizes appropriate to the problem being analyzed. Their rapid computational time permits results to be obtained on a time scale that is useful in design studies. Important attributes of a code from a design standpoint are that they be relatively easy to use and sufficiently robust to be applied over the desired design conditions. In the turbomachinery area, the three-dimensional inviscid EULER3D code is already part of the design system, providing a single unified solution for the design of conventional and unconventional bladerows. The three-dimensional viscous HAH code is almost at that stage for conventional bladerows. Results from both of these codes were presented. In the hypersonic propulsion area, several codes are currently being exercised to determine their appropriateness for utilization in the inlet design process. Among these are the SCRAMP, SCRINT, and PEPSIS PNS codes, the NASCRIN Navier-Stokes code, and the Euler TRIAD2D code. Results from several of these codes were presented. The availability of a CRAY-XMP at GE-AEBG will accelerate the selection process.

REFERENCES

1. Holmes, D.G. and Tong, S.S., "A Three-Dimensional Euler Solver for Turbomachinery Blade Rows," ASME Paper 84-GT-79, October 1, 1984.

2. Jameson, A., Schmidt, W., et al, "Numerical Solutions of the Euler Equations by Finite-Volume Methods Using Runge-Kutta Time-Stepping Schemes," AIAA Paper 81-1259, 1981.

3. Gregory, B.A., "A Comparison of Results Obtained from the Euler Inviscid 3D Code Program (EULER3D) with Those Obtained in A Cascade Test Configuration for the E-Cubed Vane," General Electric Turbine Design and Evaluation Memo TDE 0031, December 1984.

4. Hah, C., "Navier-Stokes Calculations of Three-Dimensional Compressible Flow Across A Cascade of Airfoils With An Implicit Relaxation Method," AIAA Paper 85-0555, 1985.

5. Leylek, J., "HAH Code", GE-AEBG Memo dated August 19, 1985.

6. Krawczyk, W.J., Jr., Rajendran, N., et al, "Computational Models for The Analysis and Design of Hypersonic Scramjet Components," Paper AIAA-86-1596, presented at the AIAA/ASME/SAE/ASEE 22nd Joint Conference, Huntsville, Alabama, June 1986.

7. Curtis, J.T., "Hemisphere Viscous Shock Layer Code for Equilibrium Air," AEDC-TR-82-22, January 1984.

8. Buggeln, R.C., McDonald, H., et al, "Development of a Three-Dimensional Supersonic Inlet Flow Analysis," NASA CR 3218, January 1980.

9. Kumar, A., "Numerical Simulation of Flow Through Scramjet Inlets Using A Three-Dimensional Navier-Stokes Code," AIAA Paper 85-14, July 1985.

10. Holmes, D.G. and Lamson, S.H., "Adaptive Triangular Meshes for Compressible Flow Solutions," GE-CR&D Report CRD079, April 1986.

11. Jameson, A., and Mavriplis, D., "Finite Volume Solution of the Two-Dimensional Euler Equations on a Regular Triangular Mesh," AIAA Journal, Volume 24, No. 4, April 1986.